African Journal of Advanced Pure and Applied Sciences (AJAPAS)
Online ISSN: 2957-644X
Volume 3, Issue 2, April-June 2024, Page No: 39-49
Website: *https://aaasjournals.com/index.php/ajapas/index*
معامل التأثير العربي 2023: (1.55) **SJIFactor 2023: 5.689** **ISI 2022-2023: 0.557**

Characterization of the Microstructure and Mechanical Properties of Austenitic Stainless Steel 304L by Utilization of Distinct Filler Materials Welded by TIG Method

Murad A. Debeski [1], Maryem M. Morghem [2*], Adel M. Faraj Daw [3], Taher M. Alabani [4], Omaima M. Alkubat [5]
[1,2,3,4,5] Libyan Advanced Occupational Center for Welding, Tripoli, Libya

[*]Corresponding author: mariammorgham@yahoo.com

Received: February 01, 2024	Accepted: March 28, 2024	Published: April 19, 2024

Abstract
Austenitic stainless steel is a type of steel that contains chromium and nickel. These steels are widely used in various engineering industries because they possess improved mechanical properties, especially at high temperatures. This study emphasizes the significance of utilizing different filler wire electrodes to enhance the microstructural morphologies and improve the mechanical properties of welded joints. The experimental setup involved joining AISI 304L plates with a thickness of 3mm using the Tungsten Inert Gas (TIG) metal arc welding process. Two types of electrodes, ER2209 and ER308, were employed. To analyse the chemical composition of the austenitic stainless steel plates, spectrometer analysis was conducted. This ensured the confirmation of the chemical composition of the plates before welding. The TIG welding process was carried out using a TIG machine with constant parameters of current and voltage
Results: the results indicated that the microstructural investigation revealed the formation of δ-ferrite and γ-austenite in the weld (welded by ER2209 and ER308 filler). The higher δ-ferrite content was found more in ER2209 weld zone. Whereas samples welded by ER308 filler showed the columnar structure in the weld zone. Relatively, The weld joint produced with ER2209 electrodes revealed optimum UTS value and YS value of 677 and 625 in N/mm^2 respectively, ER2209demonstrated better mechanical properties, while the weld joint produced with ER308 had superior ductility, also optimum hardness values of 411.9HV for HAZ and 490.72HV for Fuzion zone obtained with ER2209 electrode.
Welds with both electrodes should have better mechanical properties than the base metal. The author commented that the filler wire (ER2209) exhibited better tensile properties than ER308wire due to a sufficient amount of ferrite, allotiomorphic and austenite in the form of wedge-shaped widmanstatten and as intergranular precipitates in the weld zone were found.

Keywords: Austenitic Stainless Steel 403L, TIG Welding, ER 2209, ER308, δ-ferrite, γ-austenite.

Cite this article as: M. A. Debeski, M. M. Morghem, A. M. F. Daw, T. M. Alabani, O. M. Alkubat, "Characterization of the Microstructure and Mechanical Properties of Austenitic Stainless Steel 304L by Utilization of Distinct Filler Materials Welded by TIG Method," African Journal of Advanced Pure and Applied Sciences (AJAPAS), vol. 3, no. 2, pp. 39–49, April-June 2024.

تقييم التركيبة الداخلية والخصائص الميكانيكية لوصلات اللحام الغير قابل للصد 304L باستخدام نوعين مختلفين من الإلكترودات بتقنية TIG

مراد عياد الدبسكي [1]، مريم محمد مرغم [2*]، عادل فرج ضو [3]، الطاهر اللعباني [4]، أميمة محمد الخباط [5]
1،2،3،4،5 المركز الليبي المهني المتقدم اتقنيات اللحام ، طرابلس، ليبيا

الملخص
الفولاذ المقاوم للصدأ هو الفولاذ الكروم والنيكل الدي يستخدم على نطاق واسع في معظم الصناعات الهندسة نظرًا لخصائصه الميكانيكية المحسنة في درجات الحرارة المرتفعة. تسلط هده الورقة الضوء على أهمية استخدام أقطاب أسلاك الحشو المختلفة الأشكال المجهرية وتحسين الخواص الميكانيكية للصلب 304L منخفض الكربون لذلك تم لحام ألواح الصلب بتقنية لحام الغاز الخامل وبسمك 3ملم بواسطة الالكترودات المختلفة وباستخدام تحليل مقياس التحليل الطيفي لتحليل التركيب الكيميائي للأواح المستخدمة لتأكيد التركيب الكيميائي للصلب الاوستنيتي، وبعد إجراء عمليات اللحام بمعاملات تابثة لتقنية الغاز الخامل وباستخدام المجهر الضوئي وآلة إختبار الشد لتحليل سلوك الوصلات الملحومة تبين إلى أن التحقيق في البنية المجهرية عن وجود الفريت وبيتا المجهرية في الوصلات الملحومة بسلك (ER2209) وأن قيمة المقاومة وإجهاد الخضوع حوالي 677 و625 نيوتن/مم^2 على التوالي وبالتالي أظهرت النتائج أن القطع الملحومة بسلك (ER2209) افضل ميكانيكيا من التي تم لحامها بسلك (ER308) ولكن الوصلات التي تم لحامها بالنوعين المختلفين من الإلكترودات دات خصائص أفضل ميكانيكيا من المعدن الأساس .

الكلمات المفتاحية: الحديد غير قابل للصدأ(304) منخفض الكربون , لحام الغاز الخامل TIG ,سلك اللحام),(ER2209), (ER308),(طور الدلتا(δ) ,طور الاوستنيت (γ).

1. Introduction

Austenitic stainless steels refer to a type of steel that contains chromium and nickel. These steels are widely used in various engineering industries due to their superior mechanical properties, especially at high temperatures [1, 2]. Due to its outstanding resistance to corrosion in seawater environments [3], Austenitic Stainless Steel (ASS) AISI 304L is extensively utilized in defence and nuclear science. Compared to stainless steel 304, stainless steel 304L contains lower levels of carbon, making it more weldable. This advantageous characteristic of ASS 304L is attributed to the presence of molybdenum, which helps prevent chloride-induced corrosion. Furthermore, the lower carbon content in 304L enhances its wear and friction properties and reduces susceptibility to intergranular corrosion [4, 5]. Therefore, when welding, the selection of appropriate filler materials or electrodes becomes a crucial parameter to achieve the desired properties in the weld. . Based on the microstructural features of the fusion zone (FZ), base metal (BM), and heat-affected zone (HAZ), the weld joint's performance determines when it is in use. The HAZ, however, becomes more crucial than BM and FZ because of the differentially feature microstructures in the HAZ that occur from heat cycles and correspond to various mechanical characteristics. The electrode composition has the potential to impact the microstructural properties of the weld joint

[6, 7], by carefully selecting suitable electrode properties [8], it is possible to minimize welding defects such as solidification cracking, porosity, and poor weldability in the weld metal. It has been reported that a small amount of delta (δ) ferrite present in the weld zone can help overcome these B defects. The quantity of ferrite content in the weld plays a crucial role in determining the service requirements for the fabricated components. Although different metals can be welded in many ways, it is an advantageous way to obtain high-quality welds with TIG weld, smooth surface and excellent weld, In this study, we will use two pieces of AISI304L Stainless Steel and welding by TIG technique. During the assembly, two additional wires, Duplex stst ER 2209, and ER308 we will use. After joining with these different additives metals microstructure, micro hardness and tensile tests will performed on the joined materials to determine the effects on the weld zone, and microstructure studies. The major types of welding parameters are current (affecting the heat input), voltage usage, polarity, welding filler type, welding filler size, are length, electrode angle, arc travel speed and welding technique [8]. In general, austenitic stainless steel (ASS) produced through casting consists of a single phase. However, the weld of ASS exhibits two phases. This is because the rapid welding process does not allow sufficient time for the phase transformation of δ-ferrite to austenite, resulting in the presence of residual δ-ferrite in the microstructure [9, 10]. Moreover, the shape, size, and fraction of δ-ferrite in the weld are influenced by the ratio of chromium (Cr) and nickel (Ni) equivalents, which are determined by the chemical composition of the filler metal and the heat input during welding [11, 12, 13, 14]. As a result, the microstructure of the welded portion of ASS differs significantly from that of the base material [15, 16, 17]. The presence of δ-ferrite in the microstructure has a notable impact on the material properties. Chuaiphan et al. [9] conducted a study on SUS 216 SSe ER 316 SS, examining the influence of microstructural changes induced by varying the heat input on the mechanical properties and chemical corrosion.

Lu et al. [18] According to the author's conclusion, austenitic weld metal is mostly made up of widmansatten austenite in a ferrite matrix and allotrimorphic grain boundaries. Welds using both electrodes should have greater mechanical qualities than base metal. The author noted that because there was a substantial quantity of ferrite, allotiomorphic austenite in the form of wedge-shaped widmanstatten, and intergranular precipitates in the weld zone, the filler wire (ER2209) displayed superior tensile qualities than ER308 wire.

2. Experimental Procedure:

2.1 The Material Used:

The preliminary parametric study was performed on plates welded with dimensions 250×100×3mm of SS304L austenitic stain steel st.st (EN: 1.4303, UNS S30403) and the chemical composition as received was within in the range of specification for the cast alloy. The chemistry data obtained for this alloy used in the research and the

mechanical properties are presented in the Table 1 and Table 2 respectively. The specimens were turned in a milling machine and faced to prepare the joint configuration. Square butt joints with a root gap of 1-2mm between the BM of similar weld specimens,Single pass TIG process with direct current the welding was performed in a direction perpendicular to the rolling direction of both plates as square butt joint with machined surfaces and were held firmly using fixture to prevent distortion as shown in Fig1.(a),(b). Tensile test specimens were cut using electrical discharge machining (EDM) according to the standards such as 20x200x2. Measurements of tensile test specimens as schematic are shown Figure.2.

Table 1. Chemical Composition of Austenitic Stainless Steel 304L.

Grade	C%	Mn%	Si%	P%	S%	Cr%	Ni%	N%
304L	0. 03	2	.75max	0.045max.	0.03max.	18-20max	8-12.0max.	0.1 max.

Table 2. Mechanical Specifications.

Grade	Tensile Strength (Ksi)	Yield Strength (Ksi)	Elongation%	Hardness (Brinell)	Hardness (Rockwell)
304L	70	25	40	201	90

2.2 Welding processes. After being finished the final dimensions of two AISI 304LASS plates are aged, prepared, and beveled for TIG welding using a lath machine, as seen in figure 1 (a),(b) samples welded by two different electrodes wire. Table 3 shows the chemical constitution of the ER2209Dss and ER308 wires utilized in this experiment. To enable filler metal's composition changes without requiring a high-cost production procedure, metal-cored filler wires were employed.

Table 3. Metal-cored filler wires' chemical composition (weight percentage).

Filler	C%	Si%	Mn%	Mo%	Ni%	Cr%	P%	S%	Cu% total
ER2209	< 0.03	0.9	0.5-3.5	2.5-3.5	7.5-9.5	21.5-23.5	0.03	0.03	0.75
ER308	0.08	0.3-0.65	1.0-2.5	0.75max	9.0-11.00	19.0-22.0	0.03	0.03	0.75

2-3 Evaluation of welded joint. The specimens were visually inspected and by conventional nondestructive testing, then the specimens were cut x-sectioned transverse to welding direction the specimens were prepared for metallographic examinations using standard technique. The procedure for the preparation of metallographic specimens involved(taking a cross-sectional slice of the welded region). by utilizing velvet cloth and 0.75 μm alumina slurry after polishing on emery papers (150, 320, 400, 600, 800, 1000, and 1200 grit) in succession. The final polishing was done by 0.25 μm diamond paste to achieve mirror finish. The samples were chemical- etched by reagent (100ml water, 100 ml HCl and 100ml Nitric acid) immersion etch .The configuration of the fusion zone was analyzed using a stereoscope, and optical microscopy (OM) was used to characterize the microstructure of the fusion zone. Microstructures of various zones, such as base metal (BM), heat affected zone (HAZ), and weld metal (WM), were also seen. The Micro hardness was measured across the welded joints. The measurements were carried out in accordance with applicable requirements at room temperature. Nine places, including the first and second weld metal along the thickness, had their hardness measured as well. Electric discharge machining (EDM) was used to extract five samples for tensile testing from each welded plate. The samples for tensile strength and hardness are prepared perpendicular to the direction of the weld plate in accordance with ASTMA370-07 Standards. These schematics below, Figures (2) demonstrate how these samples are made .

Figure 3(a), (b) shown Specimens Extract for Tensile test with ER2209 wire electrode and ER308wire electrode respectively.

(a) (b

Figure 1 samples welded by samples welded ER 308

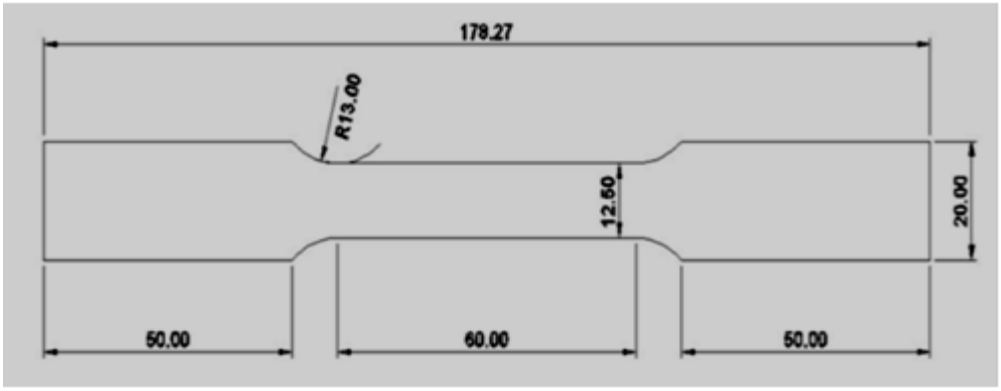

Figures (2): Standard for tensile test according A370-07

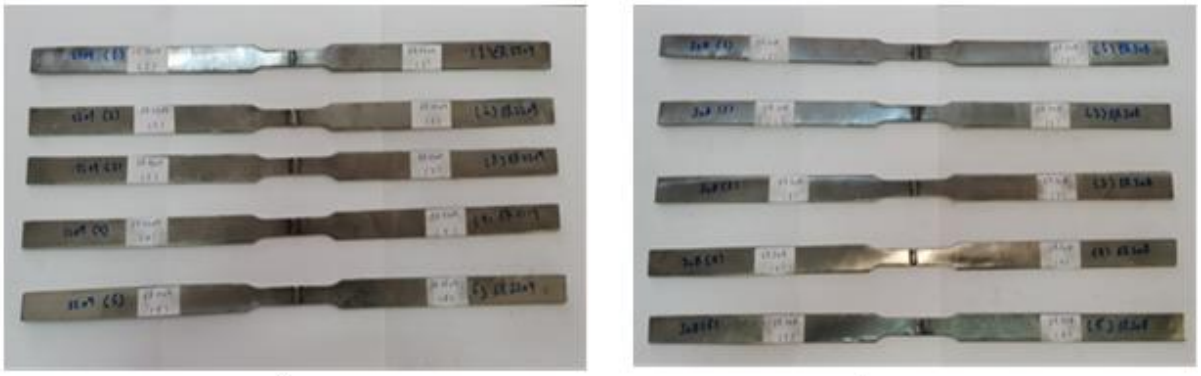

A b

Figure: 3 (a): Specimens Tensile test with ER2209, **(b):** Specimens Tensile test with ER308

3. Findings and Discussion:

3-1 Examination of the Microstructure of the Welded Samples .

3-1-1 Mode of Solidification and δ ferrite Content Estimation.

The solidification mode in the FZ is determined by the chemical composition of the filler electrode and base metal, as per to Eq. (1), (2) [19]

Cr equivalent = % Cr+%Mo+0.5%Nb+1.5%Si+2%Ti……..…...….. (1)

Ni equivalent=%Ni+30%C+0.5%Mn……..... (2)

In austenitic SSs, the solidification mode can be identified.

Using the WRC-1992 diagram, Creq/Nieq divides it into the four equations that follow.: [20].

Mode Austenite (A): L → (L+ γ) →; (Cr eq/Ni eq) <1.25……..….(3)

Austenite →ferrite mode (AF): L→ (L+γ) →) (L+ γ+δ) → (γ+δ) ;…..(4)
1.25 < (Cr eq/Ni eq) < 1.48
Ferrite →Austenite mode (FA): L→ (L+δ) → (L+δ+γ) →γ+δ; ……..…... (5)
1.48< (Creq/Nieq) <1.95
Ferrite mode (F): L→ (L+δ) →δ→ (γ+δ); ……..…… (6)
(Creq/Nieq)>1.95.

Taking into account the fillers' chemical constituents as indicated in Table (3) , the Cr eq. and Ni eq. were calculated and their respective locations are shown in Figure 4 The solidification mode of all the weld electrode ease evaluated by Cr eq and Ni eq ratio and plotted on the pseudo-binary diagram as shown in Figure(4)
In the present study, the calculated value of Cr eq. is 20.2%, the Ni eq is 11.9, and the Cr eq/Ni eq=20.2/11.9=1.697 therefore is found to be ferrite –Austenite mode
L→ (L+δ) → (L+δ+γ) →γ+δ, 1.48< (Creq/Nieq) <1.95 as per equation (5)
So according to the equations mode of solidification of ER 308 is
1.48< (1.697) <1.95.
The solidification mode of ER2209, Cr eq was=28.35, Nieq=12.15, Creq/Nieq=2.33
So according to the above equation, the solidification mode of ER2209SS is Ferrite mode
Ferrite mode (F): L→ (L+δ)→δ→(γ+δ),(Creq/Nieq)> 1.95 as per equation No. (6).

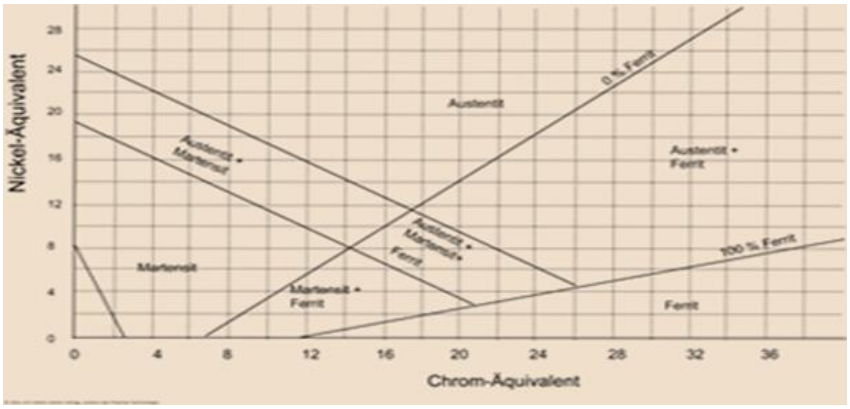

Figure 4: Schaeffler diagram for predicting welding microstructure [20].

3-2 Microstructural evaluations

I. **Microstructural investigations** are applied . For each specimen, there is base metal (BM), fusion zones (FZ), and heat affected zones (HAZ). The optical microstructure of the base is depicted in Figures 5 (a) and 5 (b). the microstructure is made up of entirely austenitic structures with twin-equiaxed grains, and no further precipitates were found there. The sample's optical microstructure, which was filled with ER2209ss filler, is mostly made up of austenite (γ) and dendritic structure (δ-ferrite); the latter is found in the form of lathy and vermicular ferrite.

II. Microstructure of Fusion Zone.

In general, the fusion zone's microstructure differs greatly from that of the base metal. This is partially caused by composition changes resulting from the base metal's dilution with the filler metal that is often employed in arc welding, as well as from the interaction of the molten metal with the ambient air. In this regard, [21] states that the zone of fusion typically had larger concentrations of C and N gamma stabilizers, which encouraged the creation of the gamma phase at high temperature and the subsequent quick cooling to martensitic. The morphology and size of the grains may have also varied significantly in the fusing zone. Because of the heat differential, large columnar grains were frequently seen in the fusion zone. The optical microstructure of the sample welded by ER2209ss filler is illustrated in Figure 6(a); it is mostly composed of austenite (γ) and dendritic structure (δ-ferrite), with the latter occurring as lathy and vermicular ferrite. The optical microstructure of the sample welded using ER308 filler is depicted in Figures 6(b, c); this microstructure is made up of columnar dendritic structure. The fundamental cause of this structure's creation is the alloying element's presence (Fe, Cr, and Ni). Due to the reduced tendency of Fe, Cr, and Ni to segregate in the intergranular and interdendritic areas, a fully columnar structure is produced. The columnar growth of FZ was seen for both electrodes, as per the Schaeffler diagram in Figure (4) Additionally, the skeletal morphology of δ-ferrite transformed into a lathy morphology, which can be attributed to constrained diffusion during the δ → γ changes. In the FZ, the formation of -ferrite in the form of a lathy and skeletal morphology, during low heat input process, a faster cooling rate and subsequently more amount of -ferrite retained in the FZ.

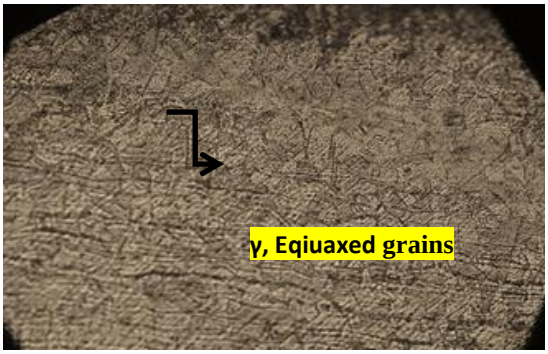

(a)

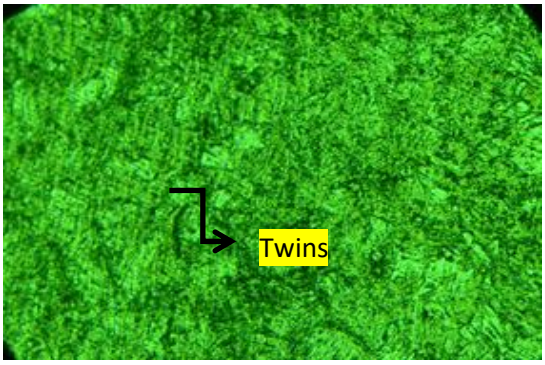

(b)

Figure 5 (a): Microstructure of base metal welded by ER308 Mag200x.

(b) Microstructure of base metal 500x welded by ER 2209

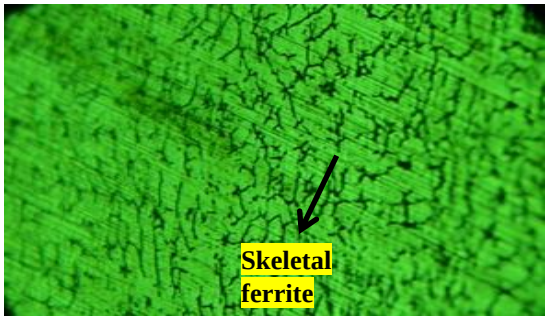

,

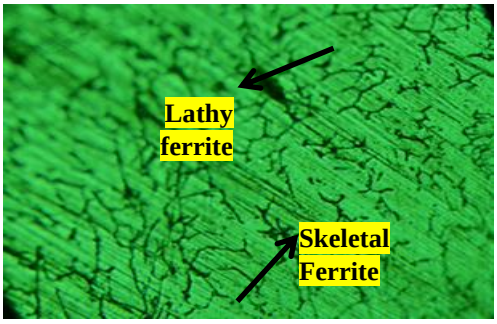

Figure 6 (a) : Fusion zone of welded joint by ER 2209 with Mag.500x

(b) Fusion zone of welded joint by ER308 with Mag. 500x

III. Microstructures of heat affected zones in heat affected zone (HAZ):The Figure 7(a,b) illustrates the observation that the acquired grain coarsening on ER2209 was significantly more pronounced. The zones adjacent to the FZ in both weldments are referred to as PMZ and HAZ, respectively. The heat input during welding had a significant impact on the HAZ. It was also noted that the weld morphology produced by using ER2209 electrode differed significantly from that of ER308 due to changes in electrode composition. Growth of cells and columns Due to ferrite grain size and ER2209, three distinct features were observed: allotrimorphs, also known as grain boundary austenite (GBA), widmanstatten (WA), a needle-shaped structure with a higher length-to-width ratio, and intra-granular austenite (IGA)[23]. While lath ferrite and skeletal ferrite were seen in the weld zone with ER308, the structure primarily consists of a dendritic structure; the production of skeleton ferrite was claimed to be caused by the rejection of Ni from the ferrite phase and Cr from austenite [24]. Conversely, higher ferrite former elements are produced by lath ferrite than by skeletal ferrite, which is created as a result of constrained diffusion and/or a distinctive cooling rate during welding [25, 26]. The main ferrite had a skeletal ferrite shape and the computed (Creq/Nieq) ratio was 1.69 as discussed above because the electrode had a higher Ni and a lower Cr, Mo content (a lower Creq/Nieq ratio) than E2209.

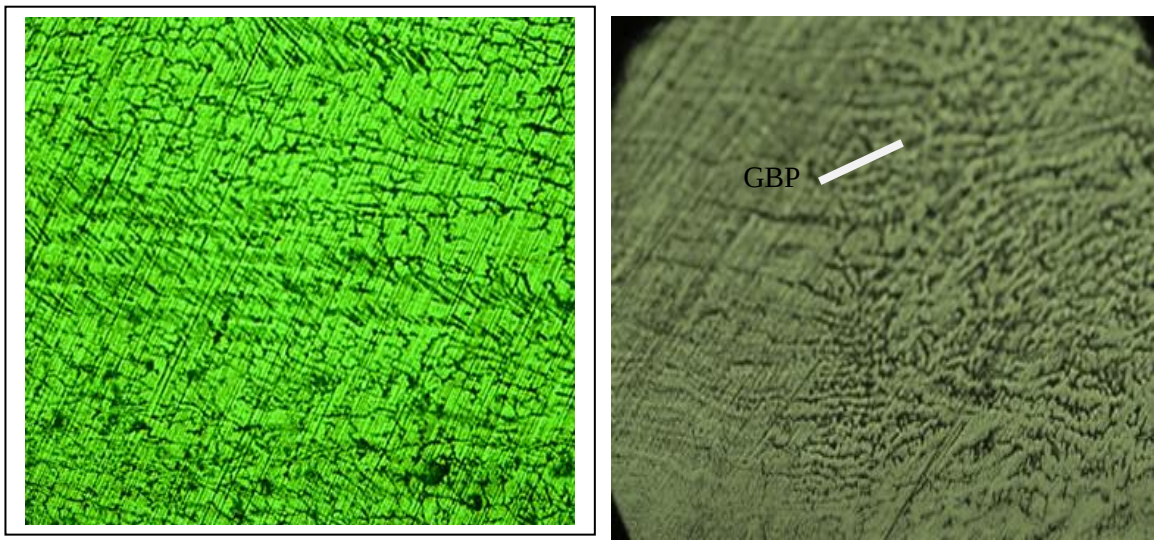

Figures 7 (a) : HAZ microstructures by ER 2209, 200X (b) HAZ microstructures by ER 308, 200X

4. Mechanical Properties.

4.1 Micro hardness studies. Figure 8 displays the findings of the microhardness measurement that was conducted across the FZ, HAZ, and BM zones. The microhardness value of HAZ is found to be lower than that of FZ for both weldments; that finding may be the result of carbon segregation.

The microhardness profile results showed that the fusion zone's microhardness values varied (490.72HVaverage, 439.55HVaverage) for ER2209 and ER308, respectively. Because of the previously indicated differences in electro decomposition, the solidification mechanism, shape, and distribution of micro-constituents in the resulting FZ could be responsible for this variation in weld hardness .In contrast to ER308, ER2209weld solidifies in the (F) mode with a greater Cr eq or Creq/Nieq ratio. Higher the Cr eq, it was reported, the higher the micro hardness (37.38HV).Nonetheless, micro-constituent elements like nickel depress microhardness, whereas nitrogen (interstitial solid solution, Cr, and Mo) raises microhardness because ER2209 has a higher nitrogen content than ER308, which in turn leads to a higher ferrite content and higher microhardness.

Due to variations in the temperature gradient, the average hardness of HAZ was 402 Hv for ER308 and 411.9 Hv for ER2209. Nonetheless, the micro-hardness profiles in the UMZ section on the 304L side increased (376.37Hv, 386.22Hv). This trend was almost identical (HV), and ferrite content was directly correlated with the results for both ER2209 and ER308L, respectively. The morphology, thermal gradient, and ferrite content were the reasons for this hardness Due to variations in the temperature gradient, the average hardness of HAZ was 402 Hv for ER308 and 411.9 Hv for ER2209. Nonetheless, the micro-hardness profiles in the UMZ section on the 304L side increased (376.37Hv, 386.22Hv). This trend was almost identical (HV), and ferrite content was directly correlated with the results for both ER2209 and ER308L, respectively. The morphology, thermal gradient, and ferrite content were the reasons for this hardness profile.

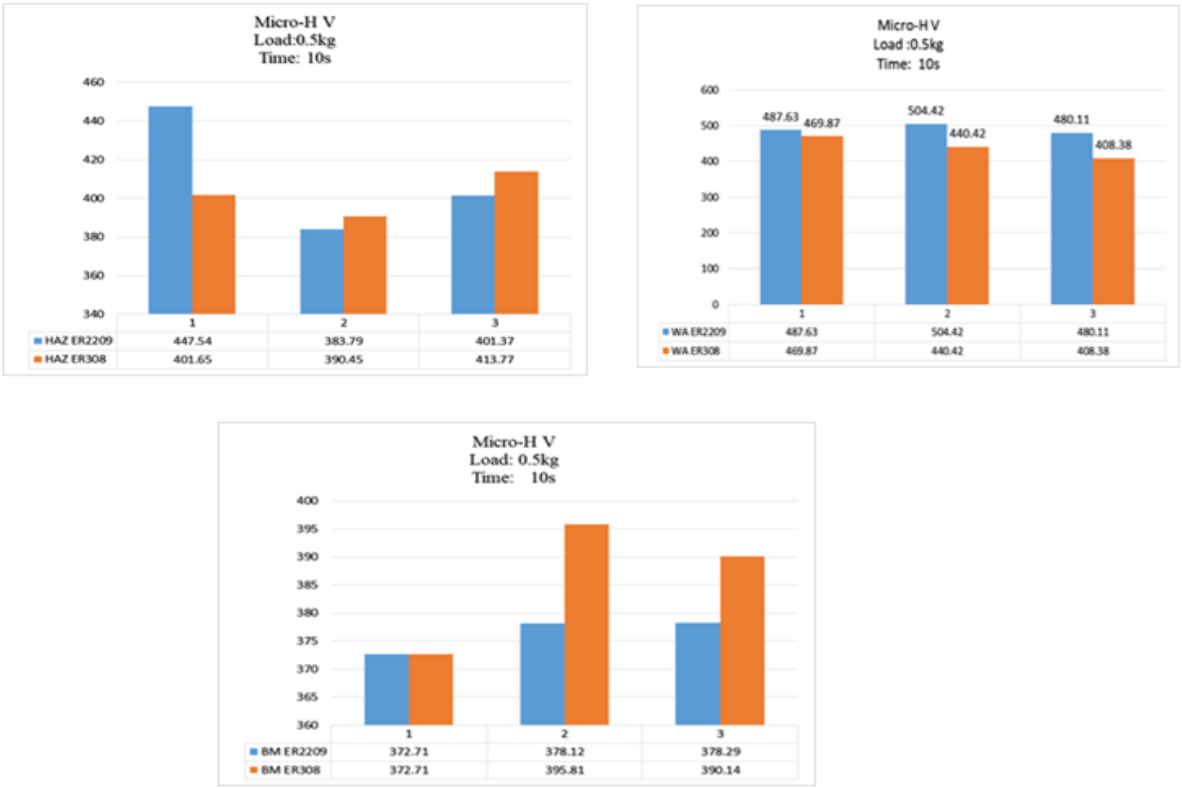

Figure 8: Comparative results of micro hardness measurements for different zones for welded joints by ER 2209, ER308

(a) **(b)**

Figure 9: Samples Tensile Tests: (a) with (ER2209), (b) with ER 308 Electrode

4-2 Tensile Test results

A ZWICK 1000 machine was used to test the tensile strength at room temperature and on a scale of 10 tons. In Figure 10. (average value is presented of two tested specimens of both electrodes) the test specimen is tensile tested to assess the quality of tensile strength of 304L steel produced by TIG welding with ER2209 and ER308 electrodes and current of 70A. The 304L BM side sustained a tensile specimen fracture, indicating that the weld connection was strong enough. For both electrodes, the mode of fracture was ductile; the tensile strength obtained for ER2209 was 646 MPa, while for ER308, it was 553.2 MPa. Because ER 2209's Cr eq. was higher, it had a better tensile strength[27] Figure (10) illustrates bar chart of the Comparison of Tensile Strength in the Weld Metal for both electrodes

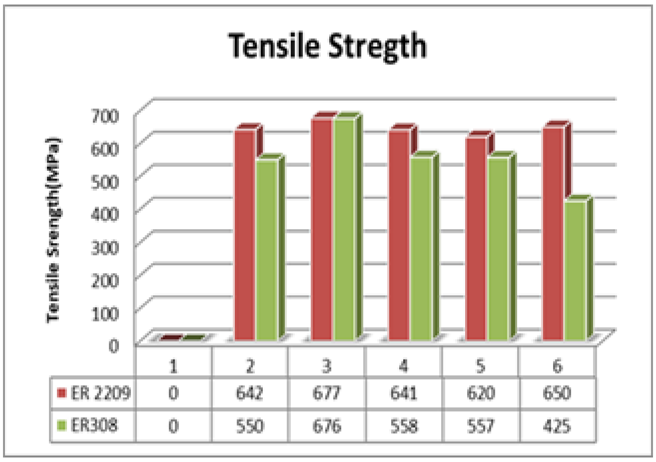

Figure 10: Illustration bar chart of the Comparison of Tensile Strength.

Appendix: Tensile tests Results of welded joints by ER2209and ER308

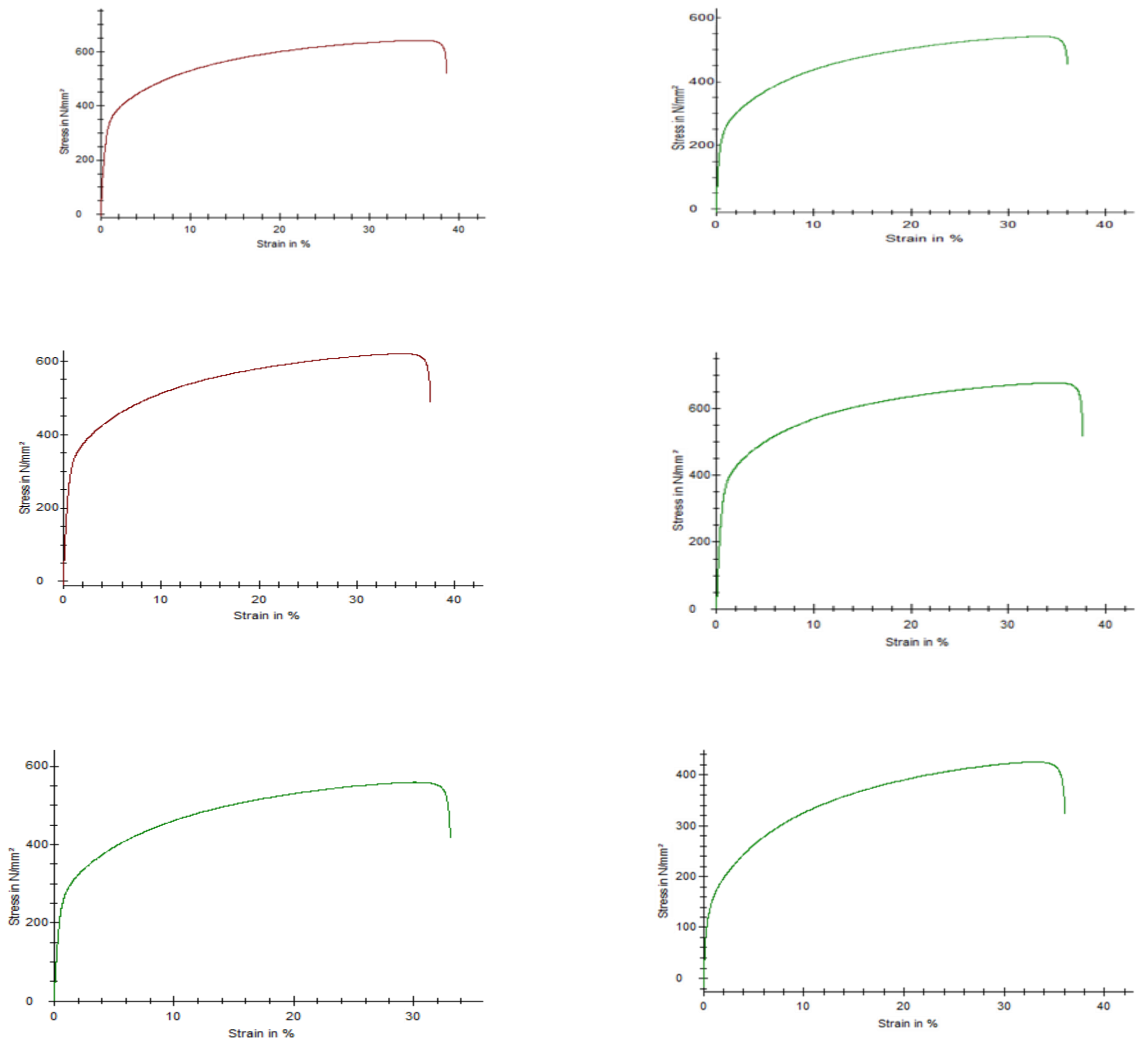

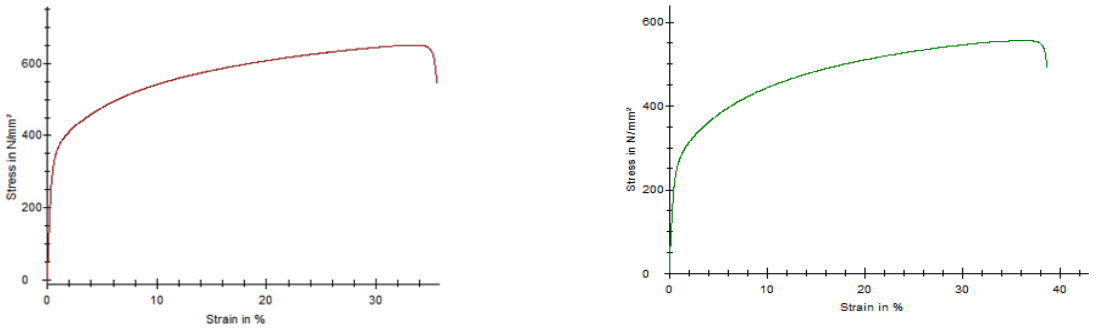

Figure 11: Tensile Strength of Weld Metal After Different Types of Electrodes(ER 2209), b. (ER 308).

4. Conclusions

The following are the findings from this study:

- The austenite matrix with varying volume proportions of δ-ferrite makes up the microstructures of the ER 2209 and ER 308 HAZs.
- The microstructures of HAZs exhibit inclusions, the development of chromium carbides (white patches), and precipitates (black, small dots).
- The ferrite composition varied significantly because ER2209 was a ferrite-austenite mode weld,
- . When using ER2209 instead of ER308, the ideal hardness value was achieved.
- The tensile test results verified that both weldments experienced a ductile fracture; however, the weldments that used ER2209 had a greater ultimate tensile strength than the ER308 weldments.
- ER2209 and ER308 electrodes yielded the best tensile properties (UTS and YS), respectively.

5. References

[1]-Srinivasan N, Kumaran S S and VenkateswarluD2019 Effects of in-grain misorientation developments in sensitization of 304 L austenitic stainless steels Mater. Res. Express 6 016551.
[2]- Su Y, ZhaoGY, Zhao YG, Meng J B and LiCX2020 Multi-objective optimization of cutting parameters in turning AISI 304 austenitic stainless steel Metals 10 217.
[3]. Gupta AK, Krishnamurthy HN, Singh Y, Prasad KM, Singh SK. Development of constitutive models for dynamic strain aging regime in Austenitic stainless steel 304. Mater Des 2013;45:616-27.
[4]. Wang XY, Li DY. Mechanical, electrochemical and tribological properties of nano-crystalline surface of 304 stainless steel. Wear 2003;255:836–45.
[5]. Iordachescu, M., Ruiz-Hervias, J., Iordachescu, D., Valiente, A. and Caballero, L. (2010) Thermal Influence of Welding Process on Strength Overmatching of Thin Dissimilar Joints. Welding in the World , 65, 201-209.
[6]. Das CR, Bhaduri AK, Srinivasan G, Shankar V, Mathew S. Selection of filler wire for and effect of auto tempering on the mechanical properties of dissimilar metal joint between 403 and 304L(N) stainless steels. Journal of Materials Processing Technology. 2009;209(3):1428-1435.
[7]. Ramkumar KD, Oza S, Periwal S, Arivazhagan N, Sridhar R, Narayanan S. Characterization of weld strength and toughness in the multi-pass welding of Inconel 625 and Super-duplex stainless steel UNS S32750. Ciência & Tecnologia dos Materia is. 2015;27(1):41-52.
[8]. N. Moslemi, N. Redzuan, N. Ahmad, T.N. Hor, Effect of current on characteristic for 316 stainless steel welded joint including microstructure and mechanical properties. Procedia CRIP. 26, 560–564 (2015)
[9]. Chuaiphan W, Srijaroenpramong L. Microstructure, mechanical properties and pitting corrosion of TIG weld Joints alternative low-cost austenitic stainless steel grade 216. Journal of Advanced Zhao L, Wei S, Wu D, Gao D, Lu S. d-ferrite transformation mechanism and its effect on mechanical properties of 316H weld metal. J Mater Sci Technol 2020; 57:33e42.
[10].Zhao L, Wei S, Wu D, Gao D, Lu S. d-ferrite transformation mechanism and its effect on mechanical properties of 316H weld metal. J Mater Sci Technol 2020; 57:311.Chuaiphan W, Srijaroenpramong L. Microstructure, mechanical properties and pitting corrosion of TIG weld
[11]. Joints alternative low-cost austenitic stainless steel grade 216. Journal of Advanced Joining Processes 2020; 2:1000273e42.
[12]. Li Y, Luo Y, Li J, Song D, Xu B, Chen X. Ferrite formation and its effect on deformation mechanism of wire arc additive manufactured 308 L stainless steel. J Nucl Mater 2021:550.

[13]. Kianersi D, Mostafaei A, Amadeh AA. Resistance spot welding joints of AISI 316L austenitic stainless steel sheets: phase transformations, mechanical properties and microstructure characterizations. Mater Des 2014; 61:251e63.
[14]. Khuenkaew T, Kanlayasiri K. Resistance spot welding of SUS316L austenitic/SUS425 ferritic stainless steels: weldment characteristics, mechanical properties, phase transformation and solidification. Metals 2019; 9. https:// doi.org/10.3390/met9060710.
[15]. Li X, Gong B, Deng C, Li Y. Effect of pre-strain on microstructure and hydrogen embrittlement of K-TIG Welded austenitic stainless steel. Corrosion Sci 2019;149:1e17. https://doi.org/10.1016/j.corsci.2018.12.018.
[16]. Li X, Gong B, Deng C, Li Y. Failure mechanism transition of hydrogen embrittlement in AISI 304 K-TIG weld metal under tensile loading. Corrosion Sci 2018;130:241e51. https:// doi.org/10.1016/j.corsci.2017.10.032.
[17].Nam TH, An E, Kim BJ, Shin S, Ko WS, Park N, Kang N, Jeon JB. Effect of post weld heat treatment on the microstructure and mechanical properties of a submerged-arc-welded 304 stainless steel. Metals 2018;8:26. https://doi.org/10.3390/ met8010026.
[18]. Lu WF, Huang JY, Yung TY, Chen TC, Tsai KC. Effects of dendrite axis and fusion boundary on stress corrosion cracking of ER 308 L/SS 304L welds in a high-temperature water environment. Int J Pres Ves Pip 2020;179:103940. https://doi.org/10.1016/j.ijpvp.2019.103940.
[19] D.J. Kotecki, T.A. Sievert, WRC-1992 constitution diagram for stainless steel weld metals: a modification of the WRC-1988 diagram. Weld. J. 71, 171s–178s (1992).
[20] K. Rajasekhar, C.S. Harendranath, R. Raman, S.D. Kulkarni, Microstructural evolution during solidification of austenitic stainless steel weld metals: a color metallographic and electron microprobe analysis study. Mater Charact. 38, 53–65 (1997).
[21]F. Karci, R. Kacar, S. Gündüz, The effect of process parameter on the properties of spot welded cold deformed AISI 304 grade austenitic stainless steel. J. Mater. Process. Technol. 209, 4011–4019 (2009).
[22] R. Badji, M. Bouabdallah, B. Bacroix, C. Kahloun, B. Belkessa and M. Halim: Mater. Charact. 59 (2008) 447–453.
[23]R. Kacar: Mater. Des. 25 (2004) 1–9.
[24] J. A. Brooks, J. C. Williams and A.W. Thompson: Metall. Trans. A 14 (1983) 1271–1281.
[25] J. C. Lippold and D. J. Kotecki: Welding Metallurgy and Weldability of Stainless Steel, (John Wiley & Sons, 2011) pp. 1–357.
[26]R. Saluja and K.M. Moeed: Int. J. Mech. Eng. Technol. 5 (2014) 36–43.
[27] H. Y. Liou, Y. T. Pan, R. I. Hsieh and W. T. Tsai: J. Mater. Eng. Perform. 10 (2001) 231-241.